

A constrained optimization approach to nonlinear system identification through simulation error minimization

Vito Cerone, Sophie M. Fosson, Simone Pirrera, Diego Regruto*

Abstract

This paper proposes a novel approach to system identification for nonlinear input-output models by minimizing the simulation error and formulating it as a constrained optimization problem. This method addresses vanishing gradient issues, enabling faster convergence than traditional gradient-based methods. We present an algorithm that utilizes feedback-linearization controlled multipliers optimization and provide a theoretical analysis of its performance. We prove that the algorithm converges to a local minimum, and we optimize the computational efficiency by leveraging the problem structure. Numerical experiments illustrate that our approach outperforms gradient-based methods in computational effort and accuracy.

1 Introduction

System identification is the science of learning models of dynamical systems using experimental data. From a mathematical perspective, this process involves selecting a model class and estimating its parameters by solving an optimization problem. For further reading, see works by [Ljung, 1999], [Bohlin, 2006], and [Milanese et al., 2013].

Most approaches to system identification rely on prediction error minimization, which involves identifying the model parameters by minimizing the difference between the measured output and the one-step-ahead prediction provided by the model. Prediction error minimization methods are consistent, meaning that the parameter estimates converge to the true value as the amount of data increases, under the crucial assumption that the selected model classes for both the system and the noise are correct (see [Ljung, 1999]). However, if these assumptions are not satisfied, prediction error minimization methods may yield models that exhibit low accuracy when used to simulate the system. See [Zhang, 2004] and [Piroddi, 2008] for a detailed discussion on this topic.

A viable alternative is to formulate the parameter estimation problem as the minimization of the simulation error, defined as the difference between the measured output and the output predicted by the model over the entire data set. This approach, known as *simulation error minimization* (SEM), yields consistent estimates regardless of the measurement

noise model; see [Söderström and Stoica, 1982] and [Farina and Piroddi, 2010].

The primary disadvantage of SEM is the difficulty in solving the optimization problem, which is non-convex in general. Notably, even when the system is linear time-invariant, the resulting SEM problem is non-convex and polynomial; see, for example, [Cerone et al., 2012] and [Cerone et al., 2023].

In the general case of nonlinear systems, the SEM problem is a generic differentiable non-convex minimization problem, and the standard approach to its solution relies on gradient-based optimization. Among these methods, we mention the gradient-descent, pseudo-second-order algorithms, and methods based on extended Kalman filters. We refer the reader to [Ruder, 2016] for an exhaustive overview. All gradient-based methods require computing the gradients of the output samples with respect to the model parameters. These gradients depend recursively on each other, generating a dynamic dependence. [Narendra and Parthasarathy, 1991] explicitly exploit this relation to define an estimation algorithm. Alternatively, we can compute the gradients in closed form or by automatic differentiation; see [Baydin et al., 2018] for a recent survey. The backpropagation through time (BPTT) algorithm introduced in [Williams and Zipser, 1990] has recently gained popularity for identifying nonlinear systems described through recurrent neural networks. For further reading, see [Medsker and Jain, 1999] and [Salem, 2022].

The dynamic relation between the gradient samples leads to vanishing and exploding gradient issues. In essence, these problems stem from the stability of the dynamical system relating the gradients to each other. If the system is stable, the contribution of past samples vanishes; if unstable, the gradients diverge. Practical implications of these issues include convergence to inaccurate estimates and slow convergence or instability of the identification algorithm. See [Bengio et al., 1994] and [Pascanu et al., 2013] for more details.

When dealing with gray-box SI, gradient-based SEM often results in severely inaccurate estimates; see, e.g., [Parrilo and Ljung, 2003] and [Prot and Mercère, 2020]. In black-box SI, the standard solution to attenuate the vanishing gradient problem is to define ad hoc models like long-short-term memory (LSTM) or gated recurrent unit (GRU) networks. However, LSTM and GRU are prone to overfitting, and their training is energy- and time-consuming.

Alternatives to gradient-based optimization are limited. While meta-heuristic approaches, such as those proposed by [Blanco et al., 2001] and

*Corresponding author S. Pirrera. Tel. +39-3458029965, email: simone.pirrera@polito.it

[Bas et al., 2022], exist, they are often avoided due to their high computational complexity and lack of theoretical guarantees. Additionally, we reference the work of [Piroddi and Spinelli, 2003] and [Farina and Piroddi, 2011], which employ prediction error minimization and a-posteriori simulation error evaluation. However, these methods are only applicable to linearly parametrized models. [Adeoye and Bemporad, 2024] introduce a method using constrained optimization and sequential quadratic programming (SQP). However, since SQP is a second-order algorithm that requires computing large Hessian matrices, approximations are adopted.

This paper proposes a novel algorithm to address SEM identification of nonlinear input-output (NIO) models. We formulate the identification problem as a *constrained optimization* problem. The cost function accounts for the simulation error and the constraints for the structure of the model. This approach avoids recursively computing the output variables' gradients over time, thus eliminating any vanishing or exploding gradient issues at the cost of introducing additional optimization variables. To solve the optimization problem, we resort to the *feedback linearization controlled multiplier optimization* (FL-CMO), which is a control-based continuous-time algorithm for equality-constrained optimization presented in [Cerone et al., 2024], and we apply Euler integration to derive a stable iterative algorithm from the FL-CMO differential equation.

This work introduces two main contributions. First, we provide a comprehensive theoretical analysis of the proposed approach. Specifically, we analyze the relation between the constrained and unconstrained SEM problem formulations, and we establish convergence guarantees for the proposed method. Additionally, we examine the algorithm's computational complexity and develop strategies to address its bottlenecks. Moreover, we show how to adapt the approach to handle noisy input data and state-space models.

The second contribution involves demonstrating the effectiveness of the proposed approach on several significant system identification problems. We focus on four key examples. The first example shows that our approach outperforms standard methods for neural NIO identification on the fluid damper benchmark. In the second example, we compare our approach with existing results on the Bouc-Wen benchmark. The third example illustrates that our method enhances accuracy and reduces training time compared to state-of-the-art neural identification techniques, specifically LSTM and GRU. Finally, in the fourth example, we address a realistic gray-box identification problem and compare our method to prediction error minimization and gradient-based SEM.

We organize the paper as follows. Section 2 formalizes the SEM identification problem and clarifies the role of the vanishing gradient issue in the related literature. In Section 3, we expand the proposed approach, formulating the problem as constrained optimization and developing the algorithm based on FL-CMO. Section 4 theoretically analyzes the developed algorithm, proving its relation with the standard formulation and its conver-

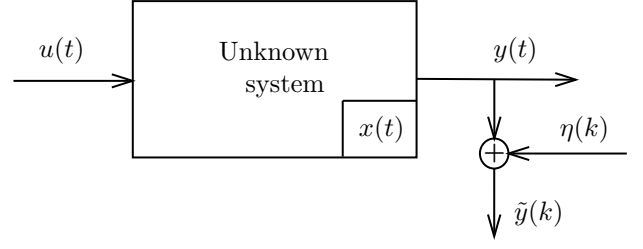


Figure 1: Block diagram of the data generation process

gence. In Section 5, we leverage the problem structure and sparse QR factorization to reduce the computational complexity. Section 5 extends the proposed approach to deal with errors-in-variables noise and state-space models. Finally, Section 7 provides numerical examples illustrating the effectiveness of the proposed approach, and Section 8 concludes the paper.

2 Problem formulation

Consider an unknown dynamical system of the form

$$\begin{aligned} x_{k+1} &= f(x_t, u_t) \\ y_t &= h(x_t, u_t) \end{aligned} \quad (1)$$

where $f : \mathbb{R}^n \times \mathbb{R}^q \rightarrow \mathbb{R}^n$, $h : \mathbb{R}^n \times \mathbb{R}^q \rightarrow \mathbb{R}^p$ are unknown functions, n is the system order, $x_t \in \mathbb{R}^n$ is the state vector, and $u_t \in \mathbb{R}^q, y_t \in \mathbb{R}^p$ are the system's input and output. As discussed in, e.g., [Conte et al., 1999], if (1) is observable, then it allows for the input-output description

$$y_t = \phi(y_{t-1}, \dots, y_{t-n}, u_t, \dots, u_{t-n}) \quad (2)$$

where $\phi : \underbrace{\mathbb{R}^p \times \dots \times \mathbb{R}^p}_{n \text{ times}} \times \underbrace{\mathbb{R}^q \times \dots \times \mathbb{R}^q}_{n+1 \text{ times}} \rightarrow \mathbb{R}^p$ is a suitable function depending on f and h .

We consider the problem of identifying a NIO model of the form

$$y_t = \mathcal{M}(y_{t-1}, \dots, y_{t-n}, u_t, \dots, u_{t-n}, \theta), \quad (3)$$

where $\mathcal{M} : \underbrace{\mathbb{R}^p \times \dots \times \mathbb{R}^p}_{n \text{ times}} \times \underbrace{\mathbb{R}^q \times \dots \times \mathbb{R}^q}_{n+1 \text{ times}} \times \mathbb{R}^{n_\theta} \rightarrow \mathbb{R}^p$ is a gray-box or black-box parametric model for ϕ .

We assume that input-output data, denoted as $\{u_t, \tilde{y}_t\}$ for $t = 1, \dots, N$, are available. Figure 1 illustrates the structure of the data-generating process. Specifically, we assume that the input u_t is known exactly, while the output measurements are corrupted by noise according to the equation $\tilde{y}_t = y_t + \eta_t$. Here, y_t represents the noise-free output, and $\eta_t \in \mathbb{R}^p$ denotes a noise sequence.

We formulate the NIO identification problem using the SEM approach; see, e.g., [Farina and Piroddi, 2010]. Accordingly, we consider the optimization problem:

$$\underset{\zeta \in \mathbb{R}^{n_\theta + pn}}{\operatorname{argmin}} \sum_{t=1}^N \|y_t(\zeta) - \tilde{y}_t\|_W^2 + \rho(\theta) \quad (4)$$

where $\zeta = [\theta^\top, y_1^\top, \dots, y_n^\top]^\top \in \mathbb{R}^{n_\theta + pn}$ is the optimization variables vector, $\|\eta\|_W \doteq \sqrt{\eta^\top W \eta}$ for some posi-

tive definite matrix $W \in \mathbb{R}^{p \times p}$, $\rho : \mathbb{R}^{n_\theta} \rightarrow \mathbb{R}$ is a differentiable regularization term, and $y_t(\zeta)$ is recursively defined by

$$y_t(\zeta) = \mathcal{M}(y_{t-1}(\zeta), \dots, y_{t-n}(\zeta), u_t, \dots, u_{t-n}, \theta), \quad (5)$$

for $t = n+1, \dots, N$.

Problem (4) generalizes the standard machine learning formulation as seen in, e.g., [Salem, 2022]:

$$\underset{\theta \in \mathbb{R}^{n_\theta}}{\operatorname{argmin}} \sum_{t=1}^N \|y_t - \tilde{y}_t(\theta)\|_W^2 + \rho(\theta) \quad (6)$$

where $y_t(\theta)$ is the model's output given some known initial conditions. Typical assumptions include $y_t = \tilde{y}_t$ or $y_t = 0$ for $t = 1, \dots, n$ for input-output models, and $x_0 = 0$ or a random normally distributed value for state-space models. Adopting (4), we jointly estimate the initial conditions and the network's parameters, leading to a more accurate estimation.

2.1 Related literature

The standard approach to solve Problems (4) and (6) is applying gradient-based methods. Several alternatives are available in this context. The most popular approach is considering gradient-descent (GD) algorithms such as stochastic and mini-batch GD, RM-Sprop, and Adam; see [Ruder, 2016] for a comprehensive review. Alternatively, second-order and pseudo-second-order methods are adopted. Popular choices are Newton's method, Broyden-Fletcher-Goldfarb-Shanno algorithms (see [Peng and Magoulas, 2011], [Liu et al., 2018] and [Bemporad, 2024]), and methods tailored for nonlinear least-squares problems such as Gauss-Newton or Levenberg-Marquardt algorithms (see [Mirikitani and Nikolaev, 2009]).

All the approaches mentioned above require computing the gradients $\nabla_\theta y_t$, which recursively depends on $\nabla_\theta y_j$, for all $j = 1, \dots, t-1$. This dependence implicitly defines a dynamic relation between the gradient's samples. If the dynamics is stable, the contribution to $\nabla_\theta y_t$ due to $\nabla_\theta y_k$, for $k \ll t$, is negligible (vanishing gradient). Conversely, $\nabla_\theta y_t$ is divergent if the dynamics is unstable. These phenomena are known as the vanishing and exploding gradient issues, respectively, and are discussed in [Bengio et al., 1994] and [Pascanu et al., 2013]. To motivate the need for our method, we begin with a simplified example that shows how the vanishing and exploding gradient issues arise in a basic scenario.

Motivating example. Let's consider the following first-order linear-time-invariant model

$$y_t = \theta_1 y_{t-1} + \theta_2 u_{t-1}, \quad y_1 = 0. \quad (7)$$

The model's output sample at time t is given by

$$y_t = \sum_{k=1}^{t-1} \theta_1^{k-1} \theta_2 u_{t-k}. \quad (8)$$

Problem (6) with $W = 1$ and $\rho(\theta) = 0$ is

$$\min_{\theta \in \mathbb{R}^{n_\theta}} \mathcal{L}(\theta) = \min_{\theta \in \mathbb{R}^{n_\theta}} \sum_{t=2}^N \left(-\tilde{y}_t + \sum_{k=1}^{t-1} \theta_1^{k-1} \theta_2 u_{t-k} \right)^2 \quad (9)$$

and have optimality condition

$$\nabla_\theta \mathcal{L} = 2 \sum_{t=2}^N (y_t - \tilde{y}_t) \nabla_\theta y_t = 0, \quad (10)$$

where

$$\nabla_\theta y_t = \begin{bmatrix} \frac{dy_t}{d\theta_1} \\ \frac{dy_t}{d\theta_2} \end{bmatrix} = \sum_{k=1}^{t-1} \begin{bmatrix} (k-1)\theta_1^{k-2}\theta_2 u_{t-k} \\ \theta_1^{k-1} u_{t-k} \end{bmatrix}. \quad (11)$$

In a typical gradient descent iteration, if $|\theta_1| < 1$, the terms in the summation related to large values of k become negligible, which can lead to numerical cancellation issues. As a result, for each time step t , only few terms in the sum from Equation (11) significantly impact the update of the parameter estimate. On the other hand, if $|\theta_1| > 1$, the norm $\|\nabla_\theta y_t\|$ exponentially grows as t increases.

A practical method to mitigate the exploding gradient issue is gradient clipping, as discussed by [Ramaswamy, 2023] and the references cited within. However, the vanishing gradient problem is still unresolved in general. In black-box system identification, a standard solution is to use LSTM or GRU networks, as noted by [Salem, 2022]. These networks are designed to reduce the impact of the problem, although they do not fully solve it. Most identification algorithms unaffected by the vanishing gradient issue converge slowly and require significant computational resources.

[Adeoye and Bemporad, 2024] suggest formulating the identification problem as constrained optimization to develop a learning algorithm for recurrent neural networks by exploiting SQP. They argue that this formulation allows for the development of alternative training algorithms for neural networks and provides tools for deriving convergence results. In this work, we explore the constrained optimization approach, showing that it not only leads to the creation of new algorithms but also ensures that they are resilient to vanishing gradient issues.

3 Identification through FL-CMO algorithm

This section introduces a novel algorithm for the identification of NIO models. The method is based on the FL-CMO algorithm developed in [Cerone et al., 2024].

3.1 Constrained optimization formulation

In this section, we reformulate Problem (4) as *constrained optimization*, i.e., we solve:

$$\begin{aligned} & \underset{y_1 \in \mathbb{R}^p, \dots, y_N \in \mathbb{R}^p, \theta \in \mathbb{R}^{n_\theta}}{\operatorname{argmin}} \sum_{t=1}^N \|\tilde{y}_t - y_t\|_W^2 + \rho(\theta) \\ & \text{s.t.} \\ & y_t = \mathcal{M}(y_{t-1}, \dots, y_{t-n}, u_t, \dots, u_{t-n}, \theta) \\ & \text{for } t = n+1, \dots, N. \end{aligned} \quad (12)$$

Similar mathematical formulations can be found in [Adeoye and Bemporad, 2024], where the authors introduce a method based on inexact SQP for training RNNs. Analogous constrained optimization problems are also formulated in the set-membership identification setting (see, e.g., [Milanese and Novara, 2004], [Milanese et al., 2013] [Cerone et al., 2014]), under the typical assumption that the noise is bounded and incorporates additional inequality constraints accordingly.

We denote the optimization variables of Problem (12) as $x = [\theta^\top, y_1^\top, \dots, y_N^\top]^\top \in \mathbb{R}^{n_\theta + pN}$, its constraints as $h_t(x) = y_{t+n} - \mathcal{M}(y_{t+n-1}, \dots, y_t, u_{t+n}, \dots, u_t, \theta)$ for $t = 1, \dots, N - n$, and its cost function as $\mathcal{L}(x) = \sum_{t=1}^N \|\tilde{y}_t - y_t\|_W^2 + \rho(\theta)$. Let $\lambda \in \mathbb{R}^{N-n}$ be the vector of Lagrange multipliers. The first-order optimality conditions for Problem (12) are:

$$\nabla_x \mathcal{L}(x) + \sum_{t=1}^{N-n} \lambda_t \nabla_x h_t(x) = 0 \quad (13a)$$

$$h_t(x) = 0, \quad t = 1, \dots, N - n. \quad (13b)$$

Notice that these conditions only require computing the gradients of simple functions that do not recursively depend on other expressions. As a result, any attempt to solve (13) does not run into the numerical issues related to the vanishing gradient. Below, we demonstrate how the constrained optimization approach applies to the example discussed in Section 2.1.

Motivating example, cont. Consider the system (7). Using formulation (12), and according to conditions (13), the optimality conditions of the problem are:

$$\sum_{t=2}^N \lambda_{t-1} y_{t-1} = 0, \quad \sum_{t=2}^N \lambda_{t-1} u_{t-1} = 0 \quad (14a)$$

$$2(y_t - \tilde{y}_t) + \lambda_{t-1} - \lambda_t \theta_1 = 0, \quad \forall t = 1, \dots, N, \quad (14b)$$

$$h_{t-n} = y_t - \theta_1 y_{t-1} - \theta_2 u_t = 0, \quad \forall t = 2, \dots, N. \quad (14c)$$

where we set $\lambda_N = 0$ to ease the notation, without loss of generality. Compared to (10), the system of equations (14) contains more variables and equations: the number of variables increases from 2 to $2 + N$, and the number of equations from 2 to $2N + 1$. However, all equations are now simple bilinear functions of the unknowns x and λ , eliminating the need to compute powers of θ_1 , which are known to cause vanishing gradient problems.

In general, the formulation (12) allows avoiding vanishing and exploding gradient phenomena. In fact, the novel structure of the problem does not involve the iterative composition of the function \mathcal{M} , which led to the repeated multiplication of the gradients by the Jacobian of \mathcal{M} when using gradient methods to solve Problem (4).

3.2 Identification Algorithm Based on FL-CMO

This section briefly reviews the FL-CMO dynamics presented by [Cerone et al., 2024] and defines an iterative algorithm based on its Euler discretization.

The FL-CMO dynamics deals with equality-constrained optimization problems in the form

$$\begin{aligned} \min_{x \in \mathbb{R}^n} f(x) \\ \text{s.t. } h(x) = 0, \end{aligned} \quad (15)$$

where $f : \mathbb{R}^n \rightarrow \mathbb{R}, h : \mathbb{R}^n \rightarrow \mathbb{R}^m$ can be any differentiable, possibly non-convex, functions. The dynamics is developed through design techniques in the context of continuous-time feedback control systems, where the following equations describe the plant under control:

$$\dot{x} = -\nabla f(x) - J_h(x)\lambda \quad (16a)$$

$$y = h(x). \quad (16b)$$

The Lagrange multipliers λ serve as the input to the plant, while the optimization variables x represent the state, and the constraints define the outputs. This definition is grounded in the observation that an equilibrium point (x^*, λ^*) of (16) is a stationary point for (15) if and only if $h(x^*) = 0$; see [Cerone et al., 2024, Lemma 1]. Therefore, any feedback control system that ensures asymptotic stability and zero output regulation will inherently lead to convergence at a stationary point of (15).

Under the assumption that the Jacobian of the constraints $J_h(x)$ is full-rank for all $x \in \mathbb{R}^n$, (16) has vector relative degree $r = [1, \dots, 1]^\top \in \mathbb{R}^m$ [Cerone et al., 2024, Lemma 2] and therefore the non-interacting control problem defined in the context of feedback linearization admits a solution, as can be seen in [Isidori, 1995] and [Khalil, 2002]. Applying the technique of output feedback linearization controller design, we obtain the controller:

$$\lambda = (J_h(x)J_h^\top(x))^{-1}(J_h(x)\nabla f(x) + v) \quad (17a)$$

$$v = Ky, K > 0. \quad (17b)$$

The continuous-time closed-loop system (16)-(17) defines the FL-CMO dynamics, which (locally) converges to a solution to the constrained optimization problem (15). We refer the reader to Section 4.2 for a detailed convergence analysis.

We integrate the differential equations describing the FL-CMO dynamics through the Euler method; see [Wanner and Hairer, 1996] and [Sundnes, 2024]. Algorithm 1 below illustrates the resulting procedure.

Algorithm 1 Identification algorithm based on FL-CMO dynamics and Euler method

Require: $x_0, \epsilon_f, \epsilon_h, K, \tau$

$k \leftarrow 0$

while $\delta_x \geq \epsilon_f$ or $\|h(x_k)\| \geq \epsilon_h$ **do**

$J = J_h(x_k)$

$\delta_x = -\nabla f(x_k) - J^\top(JJ^\top)^{-1}(J\nabla f(x_k) + Kh(x_k))$

$x_{k+1} = x_k + \tau\delta_x$

$k \leftarrow k + 1$

end while

The computation of the constraints Jacobian J can utilize automatic differentiation (see, e.g., [Baydin et al., 2018]) or closed-form expressions

derived through tensor calculus rules (see, e.g., [Laue et al., 2018]). Both approaches efficiently perform this computation by leveraging parallelization.

4 Theoretical analysis

This section examines the theoretical properties of the proposed algorithm. It analyzes the connection between the first-order conditions of (12) and the stationary points of (4) and establishes the algorithm’s convergence.

4.1 Relation with the unconstrained formulation

Theorem 1 *Any solution to the first-order optimality conditions of Problem (12) is a stationary point of Problem (4).*

Proof. We denote $z = [\theta^\top, y_1^\top, \dots, y_n^\top]^\top \in \mathbb{R}^{n_\theta + pn}$ and $w = [y_{n+1}^\top, \dots, y_N^\top]^\top \in \mathbb{R}^m$, with $m = p(N - n)$. Let $h(z, w)$ denote the constraints of (12) and $J_h(z, w) = [J_{h,z}, J_{h,w}]$ its Jacobian. By construction, $J_{h,w} \in \mathbb{R}^{m \times m}$ is block-triangular with all the elements on the main diagonal being full-rank, making it invertible. Denote $G(w) = \sum_{t=n+1}^N \|y_t - \tilde{y}_t\|_W^2$ and $R(z) = \sum_{t=1}^n \|y_t - \tilde{y}_t\|_W^2 + \rho(\theta)$. The first-order optimality conditions are

$$\nabla_z R + J_{h,z}^\top \lambda = 0 \quad (18)$$

$$\nabla_w G + J_{h,w}^\top \lambda = 0. \quad (19)$$

From (19) we get

$$\lambda = -J_{h,w}^{\top,-1} \nabla_w G \quad (20)$$

and replacing (20) into (18) we get

$$\nabla_z R - J_{h,z}^\top J_{h,w}^{\top,-1} \nabla_w G = 0. \quad (21)$$

By applying the Implicit Function Theorem, and given that $h(z, w) = 0$ and $J_{h,w}$ is invertible, a function $\gamma : \mathbb{R}^{n_\theta + pn} \rightarrow \mathbb{R}^m$ exists such that $w = \gamma(z)$. Moreover, the Jacobian $J_{\gamma,z}$ of γ satisfies

$$J_{\gamma,z} = -J_{h,w}^{-1} J_{h,z}. \quad (22)$$

We now consider Problem (4), whose stationary points satisfy

$$\nabla_z G(\gamma(z)) + \nabla_z R(z) = 0. \quad (23)$$

By applying the chain rule and Equation (22), we obtain the following expression:

$$\begin{aligned} \nabla_z R(z) + \nabla_z G(\gamma(z)) &= \\ &= \nabla_z R + [\nabla_{\gamma(z)} G^\top J_{\gamma,z}]^\top = \\ &= \nabla_z R - [\nabla_w G^\top J_{h,w}^{-1} J_{h,z}]^\top = \\ &= \nabla_z R - J_{h,z}^\top J_{h,w}^{\top,-1} \nabla_w G, \end{aligned} \quad (24)$$

which is zero because of (21). \square

By construction, the constrained and unconstrained formulations share identical global optimal solutions. However, local solutions may differ. Theorem 1 emphasizes that by solving (12) in place of (4) does not introduce any additional local solution.

4.2 Proof of convergence

Theorem 2 (Convergence of Algorithm 1)

Assume that τ is sufficiently small. Any point (x^, λ^*) that satisfies the second-order sufficient conditions of Problem (12) is a locally asymptotically stable equilibrium of Algorithm 1.*

Proof. First, we observe that the assumptions necessary to apply the FL-CMO method hold:

- By construction, the problem formulation ensures that $m \leq n$, meaning the number of optimization variables is at least as large as the number of constraints.
- $\text{rank}(J_h(x)) = m$ for all x . This condition is met because $J_h(x)$ consistently maintains full-rank, as demonstrated by the argument used for the $J_{h,w}$ submatrix in the proof of Theorem 1.

Under these conditions, Theorem 4 in [Cerone et al., 2024] applies. Consequently, any point (x^*, λ^*) that satisfies the second-order sufficient conditions of Problem (12) is a locally asymptotically stable equilibrium point of the dynamics (16)-(17). Finally, the argument holds because the Euler discretization preserves the equilibrium points and their stability properties under the considered assumption on τ . \square

The assumption that τ must be sufficiently small to ensure stability closely parallels the requirement for a small learning rate in standard gradient-based optimization for unconstrained problems in machine learning. As in those settings, the value of τ must be chosen carefully: if it is too large, the algorithm diverges; if it is too small, convergence becomes slow.

5 Analysis of the computational complexity

The primary computational cost of Algorithm 1 arises from solving the system of linear equations

$$\sigma \doteq (JJ^\top)^{-1} (J\nabla f(x_k) + Kh(x_k)). \quad (25)$$

This section demonstrates that we can leverage the structure of the problem to reduce the algorithm’s computational complexity.

Suppose we use the Cholesky or QR decomposition algorithm to calculate the triangular factor R such that $JJ^\top = R^\top R$. The computational complexity of the procedure is $O(m^3)$. See [Stewart, 1998] for a detailed study of the computational complexity of these algorithms.

In the following, we present a method to solve the linear system (25) by utilizing the sparsity of J to minimize the overall computational effort. In particular, we:

1. Perform the Q-free QR decomposition of J^\top , i.e., obtaining the upper triangular factor $R \in \mathbb{R}^{m \times m}$, where an orthogonal matrix Q satisfies $J^\top = QR$. This method uses the sparse Householder algorithm described in [Davis, 2011]. By applying QR factorization, $JJ^\top = R^\top Q^\top QR = R^\top R$, making R^\top a Cholesky factor of JJ^\top .

2. Apply forward and backward substitution to solve the linear system.

In the remainder of this section, we define ϕ as the dynamical order of the NIO model and $n = n_\theta + pN$ as the number of optimization variables of Problem (12).

Theorem 3 *Using a sparse algorithm, the computational complexity of a generic iteration of Algorithm 1 is $O(m^2)$.*

Proof. We calculate the operations needed for the Householder algorithm exploiting sparsity by avoiding multiplications by zeros. Table 1 shows the count of floating-point operations (FLOPs) for each step of the Householder algorithm applied to the matrix $X = J^\top$, comparing dense and sparse cases.

To analyze the first instruction of the loop, we examine the function $[u, \nu] = \text{housegen}(x)$. This function performs the Householder reflection of its argument by computing u such that $(I - uu^\top)x = \pm \|x\| e_1$, where e_1 is the first vector of the standard Euclidean basis. For additional details, refer to [Stewart, 1998].

Algorithm 2 The *housegen* function

```

 $u = x, \quad \nu = \|x\|$ 
if  $\nu = 0$  then
     $u_1 = \sqrt{2}, \quad \text{return}$ 
end if
 $u = x/\nu$ 
if  $u_1 \geq 0$  then
     $u_1 = u_1 + 1, \quad \nu = -\nu$ 
else
     $u_1 = u_1 - 1$ 
end if
 $u = u/\sqrt{|u_1|}$ 

```

The *housegen* function is defined according to Algorithm 2. The computational cost of *housegen* is primarily driven by the calculation of $\nu = \|x\|$, $u = x/\nu$, and $u = u/\sqrt{|u_1|}$. Each of these operations involves χ FLOP products, where χ is the cardinality of x . Consequently, since x_k is constructed from the k -th to the n -th element of J^\top , this step requires $3(n - k + 1)$ FLOPs in the dense case and $3\chi(k)$ FLOPs when exploiting sparsity. Based on the structure of J^\top , $\chi(k)$ is given by

$$\chi(k) = \begin{cases} n_\theta - k + 1 + p(1 + \phi) & \text{if } k \leq n_\theta \\ p(1 + \phi) & \text{if } k > n_\theta. \end{cases} \quad (26)$$

Computing the product $U_{k:n,k}^\top X_{k:n,k+1:m}$ in the dense case requires $(n - k + 1)(m - k)$ multiplications. In the sparse case, however, $U_{k:n,k}$ exhibits the same sparsity pattern as x_k except for its first element, which consistently contributes zero to the product. By leveraging this sparsity, the number of required products drops to

$$\psi(k) = \begin{cases} \psi_1(k) & \text{if } k \leq n_\theta \\ \psi_2(k) & \text{if } k > n_\theta, \end{cases} \quad (27)$$

where, for $i = (k \bmod p) + 1$, we obtain

$$\begin{aligned} \psi_2(k) &= (p - i)p(\phi + 1) + \phi p^2 + \dots + 2p^2 + p^2 \\ &= (p - i)p(\phi + 1) + \sum_{z=1}^{\phi} zp^2, \end{aligned} \quad (28)$$

$$\psi_1(k) = (n_\theta - k + 1)(m - k) + \psi_2(k). \quad (29)$$

Equation (28) derives from the observation that the number of coinciding nonzero indices decreases by p every p columns. Similarly, Equation (29) is obtained using the same procedure while also accounting for the contributions of products involving the first $(n_\theta - k + 1)$ elements of $U_{k:n,k}^\top$.

We now compute $\zeta(k)$ representing the number of FLOPs necessary to calculate the product $U_{k:n,k}v$, where $U_{k:n,k} \in \mathbb{R}^{n-k+1}$ is a sparse vector with cardinality

$$\chi_1(k) = \begin{cases} \chi(k) & \text{if } k \leq n_\theta \\ \chi(k) + 1 & \text{if } k > n_\theta \end{cases} \quad (30)$$

and $v \in \mathbb{R}^{1,m-k}$ is possibly dense. Accordingly, the result is an $(n - k + 1) \times (m - k)$ matrix in which all rows corresponding to zero elements of $U_{k:n,k}$ are zero. As a result, the dense case requires $(n - k + 1)(m - k)$ FLOPs, whereas the sparse case requires

$$\zeta(k) = (m - k)\chi_1(k) \text{ FLOPs.} \quad (31)$$

To conclude the proof, we demonstrate the existence of constants $M > 0$ and $m_0 > 0$ such that for all $m > m_0$:

$$\left| \sum_{k=1}^m 3\chi(k) + \psi(k) + \zeta(k) \right| \leq Mm^2. \quad (32)$$

Let us evaluate each term of the sum:

$$\begin{aligned} \sum_{k=1}^m 3\chi(k) &= 3 \sum_{k=1}^{n_\theta} (n_\theta - k + 1 + p(1 + \phi)) + \\ &+ 3 \sum_{k=n_\theta+1}^m p(1 + \phi) = 3m(1 + \phi)p + \frac{3}{2}(n_\theta^2 + n_\theta) \end{aligned} \quad (33)$$

$$\begin{aligned} \sum_{k=1}^m \psi(k) &= \sum_{k=1}^{n_\theta} \psi_1(k) + \sum_{k=n_\theta+1}^m \psi_2(k) \\ &= \sum_{k=1}^{n_\theta} (n_\theta - k + 1)(m - k) + \sum_{k=1}^m \psi_2(k) \end{aligned} \quad (34)$$

Let us individually expand the two terms in equation (34) to analyze their contributions.

$$\begin{aligned} \sum_{k=1}^{n_\theta} (n_\theta - k + 1)(m - k) &= \\ &= \frac{m}{2}(n_\theta^2 - n_\theta) - \frac{n_\theta}{6}(n_\theta^2 + 3n_\theta + 2) \end{aligned} \quad (35)$$

Table 1: FLOPs count for each instruction of Housholder algorithm.

Instruction	Iterations	FLOPs - dense	FLOPs - sparse
$U = 0_{n \times m}, R = 0_{m \times m}$	1	-	-
for $k = 1, \dots, m$			
$U_{k:n,k}, R_{k,k} = \text{housegen}(X_{k:n,n})$	m	$3(n - k + 1)$	$3\chi(k)$
$v = U_{k:n,k}^\top X_{k:n,k+1:m}$	m	$(n - k + 1)(m - k)$	$\psi(k)$
$X_{k:n,k+1:m} = X_{k:n,k+1:m} - U_{k:n,k}v$	m	$(n - k + 1)(m - k)$	$\zeta(k)$
$R_{k,k+1:m} = X_{k,k+1:m}$	m	-	-
end for			

$$\begin{aligned}
 \sum_{k=1}^m \psi_2(k) &= \sum_{k=1}^m \left((p - i)(\phi + 1)p + \sum_{z=1}^{\phi} p^2 z \right) = \\
 &= \sum_{j=1}^{m/p} \sum_{i=1}^p \left((p - i)(\phi + 1)p + \sum_{z=1}^{\phi} p^2 z \right) = \\
 &= \frac{m}{p} \left(p^3(\phi + 1) - \frac{1}{2}(\phi + 1)p^2(p + 1) \right) + \\
 &\quad + \frac{1}{2}mp^2\phi(\phi + 1) = \\
 &= \frac{1}{2}mp(\phi + 1)(p + p\phi - 1)
 \end{aligned} \tag{36}$$

$$\begin{aligned}
 \sum_{k=1}^m \zeta(k) &= \sum_{k=1}^{n_\theta} (n_\theta - k + 1 + p(\phi + 1))(m - k) + \\
 &\quad + \sum_{k=n_\theta+1}^m (p(\phi + 1) + 1)(m - k) = \\
 &= \sum_{k=1}^{n_\theta} (n_\theta - k)(m - k) + \\
 &\quad + \sum_{k=1}^m (p(\phi + 1) + 1)(m - k) = \\
 &= \frac{m}{2}(n_\theta^2 - n_\theta) - \frac{n_\theta}{6}(n_\theta^2 - 1) + \frac{m^2 - m}{2}(p(\phi + 1) + 1) \\
 &= \frac{m^2}{2}(p(\phi + 1) + 1) + \\
 &\quad + \frac{m}{2}(n_\theta^2 - n_\theta - p(\phi + 1) - 1) - \frac{n_\theta}{6}(n_\theta^2 - 1).
 \end{aligned} \tag{37}$$

From above equations, we observe that (37) dominates (33) and (34). By choosing M in equation (32) to be greater than $\frac{1}{2} + \frac{1}{2}p(\phi + 1)$, the result follows. \square

Remark 1 The sparsity of J can also be exploited when computing the matrix-vector products $J\nabla f(x_k)$ and $J^\top \sigma$. Table 2 presents the FLOP count for both dense and sparse algorithms.

Table 2: FLOPs count for matrix-vector multiplications

Instruction	FLOPs - dense	FLOPs - sparse
$J\nabla f(x_k)$	$m(n_\theta + N)$	$m(n_\theta + p\phi)$
$J^\top \sigma$	m^2	$m(n_\theta + p\phi)$

We evaluate the practical implications of the achieved reduction in computational complexity through a series of numerical experiments. For this purpose, we construct a fictitious problem with $p = \phi = 2$ and measure

the time required to perform a single iteration of Algorithm 1 across varying dataset dimensions. The results demonstrate relative speedups of $1.6\times$, $3.7\times$, and $5.7\times$ for $N = 10^3$, $N = 5 \cdot 10^3$ and $N = 10^4$, respectively.

Compared to the inexact SQP method proposed by [Adeoye and Bemporad, 2024], we emphasize that the size of the matrix requiring QR factorization decreases from $(n + m) \times (n + m)$ to $m \times (n + m)$. Additionally, the iterations are exact, which significantly simplifies the analysis.

6 Extensions to Error-in-Variables and State-Space Models

This section demonstrates the application of the constrained optimization reformulation and Algorithm 1 to identification problems with a structure different from that considered in Section 3.

6.1 Errors-in-Variables Models Case

The constrained optimization approach generalizes to scenarios in which both the input and output data contain noise. In this case, the available data is represented as $\{\tilde{u}_t, \tilde{y}_t\}$, for $t = 1, \dots, N$, where $\tilde{u}_t = u_t + \epsilon_t$, $\tilde{y}_t = y_t + \eta_t$. Here, $\epsilon_t \in \mathbb{R}^q$, $\eta_t \in \mathbb{R}^p$ denote the noise components. This model is commonly referred to as the errors-in-variables (EIV) one.

We formalize this problem as solving the following optimization problem

$$\begin{aligned}
 &\underset{\theta \in \mathbb{R}^{n_\theta}, u_1 \in \mathbb{R}^q, \dots, y_N \in \mathbb{R}^p}{\text{argmin}} \sum_{t=1}^N \|y_t - \tilde{y}_t\|_{W_y}^2 + \\
 &\quad + \sum_{t=1}^N \|u_t - \tilde{u}_t\|_{W_u}^2 + \rho(\theta)
 \end{aligned} \tag{38}$$

s.t.

$$\begin{aligned}
 &y_t = \mathcal{M}(y_{t-1}, \dots, y_{t-n}, u_t, \dots, u_{t-n}, \theta) \\
 &\text{for } t = n + 1, \dots, N.
 \end{aligned}$$

where $W_y, W_u \succ 0$ are appropriate weighting matrices. When the noise in the output is expected to exceed that in the input, $W_u \succ W_y$. As W_u approaches infinity ($W_u \rightarrow \infty$), \tilde{u} becomes equivalent to u ($\tilde{u} = u$), thereby recovering the output error problem.

The theoretical analysis presented in Section 4 also applies to this case, whereas the considerations on computational complexity are different from those in Section

5 due to the different sparsity of the problem. Compared to Problem (12), which was introduced in Section 3 by considering the output-error case, the number of optimization variables increases, but the number of constraints remains unchanged. Consequently, the dimensions of the linear system (25) remain the same. Furthermore, J is still sparse, and numerical experiments demonstrate that the proposed QR decomposition offers computational benefits.

6.2 State-Space Models Case

This section examines the application of the proposed approach to the identification of state-space models. We formulate the identification problem as the equality-constrained optimization problem:

$$\begin{aligned} & \underset{\theta \in \mathbb{R}^{n\theta}, x_1 \in \mathbb{R}^n, \dots, x_N \in \mathbb{R}^n}{\operatorname{argmin}} \sum_{t=1}^N (\mathcal{M}_2(x_t, u_t, \theta) - \tilde{y}_t)_2^2 + \rho(\theta) \\ & \text{s.t.} \\ & x_{t+1} = \mathcal{M}_1(x_t, u_t, \theta), \quad t = 1, \dots, N-1, \end{aligned} \quad (39)$$

where \mathcal{M}_1 and \mathcal{M}_2 represent the models for the state and output equations, respectively. This problem formulation is highly versatile and encompasses linear systems, gray-box models, recurrent neural networks, and neural state-space models.

Problem (39) features $n(N-1)$ optimization variables. Since, in general, $p < n$ (i.e., there are fewer outputs than states), this value exceeds the NIO counterpart $p(N-n)$. For this reason, input-output models are computationally preferable when employing a constrained optimization approach. Furthermore, as shown in the next section on numerical examples, input-output models exhibit a lower susceptibility to overfitting compared to state-space ones.

7 Numerical examples

This section presents numerical examples demonstrating the effectiveness of the proposed method. The examples compare the proposed approach with established alternatives on widely used system identification benchmarks.

We focus on black-box system identification using neural networks, with most examples employing neural NIO models. In line with the notation introduced by [Sjöberg et al., 1994], we denote the neural NIO model NNOE when performing SEM identification and NNARX when applying prediction error minimization identification.

The validation metrics adopted here include the root-mean-squared error (RMSE) and the best-fit rate (BFR), defined as:

$$\text{RMSE} \doteq \sqrt{\frac{1}{N} \|\hat{y} - y\|_2^2}, \quad (40)$$

$$\text{BFR} \doteq \left(1 - \frac{\|y - \hat{y}\|}{\|y - m_y\|}\right), \quad (41)$$

where y denotes the measured validation output, \hat{y} the simulated output, and m_y the sample mean of y .

Each of the following examples will consider a different value for the parameter K , to highlight the algorithm's

robustness to its selection. The value of τ is selected via a trial-and-error procedure to ensure stability of the learning dynamics.

7.1 Fluid Damper Benchmark

This subsection examines the magneto-rheological fluid damper problem from [Wang et al., 2009]. The problem considers magneto-rheological fluid dampers, which are devices used to suppress mechanical vibrations. These dampers contain fluids whose viscosity varies in response to a control signal. The benchmark dataset was obtained by attaching the test damper to a shaker table that generates realistic vibrations. Experimental data from these tests, comprising 2000 data points for training and 1499 data points for testing, are available in MATLAB's System Identification Toolbox.

This subsection evaluates the proposed FL-CMO-based algorithm against leading alternatives for neural NIO modeling in system identification, namely NNARX identification via backpropagation and NNOE training with the Levenberg-Marquardt algorithm.

We selected a single-layer network with a dynamical order $n = 4$ and 6 neurons. The identification process involved the following methods:

1. NNARX: We trained the network using Adam stochastic gradient descent with a batch size of 32. The training algorithm was implemented in Python using TensorFlow's Keras package (see [Chollet et al., 2015]), with the network trained for 2000 epochs.
2. NNOE with Levenberg-Marquardt: We used the *nnoe* function from the NNSYD MATLAB toolbox (see [Nørgård et al., 1996]), which applies the Levenberg-Marquardt algorithm. The gradient and criterion-improvement tolerances were set to 10^{-12} , while the maximum number of iterations was set to 10^5 .
3. NNOE with the proposed FL-CMO algorithm: We set the parameters to $\tau = 2 \cdot 10^{-3}$ and $K = 1$, with a maximum of 1000 iterations and regularization $\rho(\theta) = 10^{-3} \|\theta\|_2^2$.

We repeated the identification process 10 times, with different, normally distributed, initializations of the optimization variables. Table 3 reports the mean value and standard deviation of the training times (measured in seconds) and validation BFRs across all runs for the different algorithms. The results indicate the FL-CMO algorithm requires lower computational effort compared to Adam while delivering superior performance. In contrast, the Levenberg-Marquardt algorithm significantly reduces computational effort; however, it is less reliable due to the vanishing gradient issue, resulting in poorer average performance.

The obtained results are consistent with or improve upon those reported in Table I of [Bemporad, 2022], which are based on the same dataset. Specifically, standard BPTT training with the Adam optimizer achieves a validation BFR of 85.5% for both RNN and LSTM

Table 3: Example 1. Comparison of NNARX (Adam) and NNOE (FL-CMO and Levenberg-Marquardt) identification methods.

	training time	BFR
NNOE using FL-CMO	106.68 (1.17)	88.28 (1.29)
NNOE using Levenberg-Marquardt	0.32 (0.097)	66.66 (27.14)
NNARX using Adam	176.22 (32.27)	68.14 (23.32)

models, while the extended Kalman filter approach proposed in [Bemporad, 2022] yields BFRs of 89.78% and 88.97% for RNN and LSTM, respectively.

7.2 Bouc-Wen system benchmark

This section considers the Bouc-Wen model, which is described by the dynamics:

$$\begin{aligned} m_L \ddot{y}(t) + c_L \dot{y}(t) + k_L y(t) + z(t) &= u(t) \\ \dot{z}(t) &= \alpha \dot{y}(t) - \beta (\gamma |\dot{y}(t)| |z(t)|^{\nu-1} z(t) + \delta \dot{y}(t) |z(t)|^\nu), \end{aligned} \quad (42)$$

where $m_L, k_L, c_L, \alpha, \beta, \gamma, \nu, \delta$ are real scalars. This model is extensively used to characterize mechanical hysteretic effects. The problem of performing its identification belongs to the benchmarks considered during the annual Nonlinear System Identification Benchmarks workshop. For a comprehensive description of the problem, refer to [Noel and Schoukens, 2016].

A total of 5000 data pairs for training and 5000 data pairs for validation were generated using a multisine input signal, adhering to the provided MATLAB function with its default settings. Training and validation output data were corrupted by additive Gaussian noise with a variance of $8 \times 10^{-3} \text{ mm}^2$. For testing, the data provided in the files "uval_multisine.mat" and "yval_multisine.mat" were used, which include 8192 data pairs.

We trained NNOE networks with a dynamical order $n = 3$ and two layers, varying the number of neurons from 5 to 10. Training was performed using Algorithm 1, with $\tau = 2 \cdot 10^{-3}$, $K = 10$, $\epsilon_f, \epsilon_h = 10^{-4}$ and regularization $\rho(\theta) = 10^{-3} \|\theta\|_2^2$. Among the trained networks, the model containing 8 neurons was selected, as it achieved the highest validation accuracy with a BFR index of 87.38%. The network has 145 parameters, and its training required 3000 iterations of Algorithm 1, corresponding to 3521 s of computations. The achieved BFR on the provided test set is 95.01%, demonstrating the model's generalization capabilities.

Table 4: Example 2: Comparison of several methods on the Bouc-Wen system benchmark.

Method	RMSE
[Esfahani et al., 2017]	$1.87 \times 10^{-5} \text{ mm}$
[Belz et al., 2017]	$16.3 \times 10^{-5} \text{ mm}$
[Forgione and Piga, 2021]	$4.52 \times 10^{-5} \text{ mm}$
NNOE trained by FL-CMO	$3.33 \times 10^{-5} \text{ mm}$

Table 4 presents the validation RMSE of the trained model and compares it with previously reported results on this benchmark. It is noteworthy that the obtained

NNOE model demonstrates superior accuracy compared to the method by [Belz et al., 2017] and accuracy comparable to those by [Forgione and Piga, 2021], using only 5000 training data points rather than 40960, emphasizing the data efficiency of the NNOE model. This performance can be attributed to the NNOE model's reduced parameterization, which enables effective learning from smaller datasets and mitigates the risk of convergence to poor local minima. In contrast, accuracy remains lower compared that obtained with the technique introduced by [Esfahani et al., 2017], which is designed specifically for hysteretic systems.

7.3 MIMO Wiener-Hammerstein system

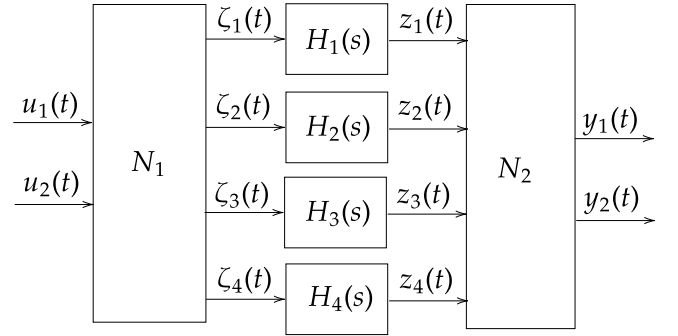


Figure 2: MIMO Wiener-Hammerstein system diagram.

In this subsection, we analyze the Wiener-Hammerstein system, which features two inputs and two outputs, as depicted in Figure 2. The input nonlinear block is described by

$$\zeta_1 = 0.2u_1u_2 - u_1 - u_2 - 0.04u_2^2(u_2 + u_1), \quad (43a)$$

$$\zeta_2 = u_1 + u_2, \quad \zeta_3 = 2u_2 - 1.3\zeta_1, \quad \zeta_4 = u_1, \quad (43b)$$

the linear blocks by

$$H_1(s) = \frac{16}{s^2 + 40s + 130}, \quad (43c)$$

$$H_2(s) = \frac{80}{s^3 + 31s^2 + 340s + 2730}, \quad (43d)$$

$$H_3(s) = \frac{30}{s + 10}, \quad H_4(s) = \frac{-10}{s^2 + 6s + 80}, \quad (43e)$$

and output nonlinear block by

$$y_1 = 7.5z_4z_1 - 51z_2 + 1.02z_4^2z_2 - 9z_1^3 \quad (43f)$$

$$y_2 = 2.7z_2z_3 - 0.729z_4z_2^2. \quad (43g)$$

We generated a training dataset by simulating the system for 35 seconds and sampling the obtained signals

with period $T_s = 0.01$ s, yielding $N = 3500$ training samples. Similarly, we generated a test dataset of 5000 samples. In both cases, the input signal is a staircase signal with stair length $T_{\text{stair}} = 100T_s$ and normally distributed amplitudes with unitary variance. We trained several NNOE models with dynamical order $n = 3$ and different neural network structures. Algorithm 1 was applied with $\tau = 0.01$, $K = 100$, $\epsilon_f = \epsilon_h = 10^{-3}$, and the maximum of 500 iterations.

We compare the results with those obtained using LSTM, GRU, and NNARX networks with various architectures. To assess model quality, we evaluated the test RMSE and BFR. Table 5 summarizes the numerical results concerning training time and accuracy, and marks in green the top-performing models within each class: NNOE(2,5), with two layers of five neurons each; LSTM(2,2), with two layers of two cells; and GRU(1,5), comprising a single layer of five cells. Figure 3 presents the validation outputs of these models.

The results indicate that the NNARX, LSTM, and GRU models require longer training times and yield lower prediction accuracy than the NNOE model. In particular, the simulation performance of the NNARX model is significantly worse. This can be attributed to NNARX training relying on PEM, whereas the other models employ SEM. At the same time, the superior performance of the NNOE model relative to LSTM and GRU stems from its higher data efficiency and the resilience of its training process to vanishing gradient issues.

Table 3 shows that a generic iteration of Algorithm 1 is more computationally intensive than a single BPTT iteration used in LSTM and GRU training. However, it requires significantly fewer iterations overall, resulting in a reduced total training time. This efficiency can be attributed to the absence of vanishing gradient issues.

7.4 Magnetic levitation system gray-box identification

We analyze the magnetic levitation system described by the continuous-time model

$$\ddot{z} = g - \frac{k_m i^2 + k_0}{mz^2}, \quad (44)$$

where z denotes the distance between the magnet and the ball, m is the mass of the ball, g denotes the gravitational acceleration, and k_m and k_0 are constants determined by the magnet's characteristics. The objective of the identification procedure is to estimate k_m and k_0 , with $m = 24.197$ g and $g = 9.81$ m/s² treated as known constants.

We simulated the differential equation (44) and collected $N = 200$ input-output data points using a sampling rate of $T_s = 10$ ms. The output data was subsequently corrupted by additive measurement noise uniformly distributed within the interval $[-5$ mm, 5 mm].

We discretized the dynamic system equation using Euler's method, resulting in the following model

$$m z_{t-2}^2 \left(\frac{z_t - 2z_{t-1} + z_{t-2}}{T_s^2} - g \right) + k_m i_{t-2}^2 + k_0 = 0. \quad (45)$$

According to the proposed approach, we evaluate the Jacobian of the constraints defined in Equation (45). Specifically, the computation requires determining the partial derivatives:

$$\frac{\partial h_t}{\partial k_m} = i_{t-2}^2, \quad \frac{\partial h_t}{\partial z_t} = \frac{m}{T_s^2} z_{t-2}^2, \quad (46a)$$

$$\frac{\partial h_t}{\partial z_{t-1}} = -\frac{2m}{T_s^2} z_{t-2}^2, \quad \frac{\partial h_t}{\partial k_0} = 1, \quad (46b)$$

$$\frac{\partial h_t}{\partial z_{t-2}} = \frac{m}{T_s^2} z_{t-2} (2z_t - 4z_{t-1} + 3z_{t-2}) - 2mgz_{t-2}. \quad (46c)$$

We applied Algorithm 1 using parameters $K = 2$ and $\tau = 10^{-3}$. For comparison, the system was also identified using the following methods:

1. Least-Squares (LS): The one-step-ahead prediction error was minimized, resulting in a linear and convex LS problem. The LS approach is widely regarded as the standard method for estimating the physical parameters of dynamical systems, particularly when the system equation depends linearly on the unknown parameters.
2. Adam Backpropagation Through Time (BPTT): The unconstrained SEM optimization problem, as outlined in Equation (6), was formulated and solved using the Adam algorithm. The loss gradient was computed through BPTT, using a learning rate of 10^{-3} , and optimization was conducted over 10^4 epochs.

We repeated the optimization 10 times for each method, using distinct, zero-mean, normally distributed initializations for the optimization variables. In Table 6, we compare the results of all three methods, selecting the best estimate among all runs for each approach. The results indicate that FL-CMO demonstrates the highest identification accuracy. Although the LS method yields an acceptable estimate, the accuracy of the k_0 parameter is one order of magnitude lower than that of the FL-CMO approach. Conversely, the Adam BPTT method produces inaccurate estimates for both parameters. We explain these results by observing that, although both FL-CMO and Adam BPTT are based on SEM, Adam BPTT suffers from the vanishing gradient issue.

8 Conclusions

This study investigates system identification for non-linear input-output (NIO) models by formulating the simulation error minimization (SEM) problem as a constrained optimization task. Through an illustrative example, we demonstrate that this formulation effectively avoids vanishing-gradient issues, which commonly hinder convergence in traditional SEM approaches. To solve the constrained problem, we introduce a novel identification algorithm that integrates feedback linearization controlled multipliers optimization (FL-CMO) dynamics with Euler method, enabling efficient and accurate model estimation.

Table 5: Example 3: Comparison of several networks.

NNOE network				NNOE Training: FL-CMO algorithm (CPU)					NNOE Validation			
order	layers	neuron/layer	# param.	RMSE y_1	RMSE y_2	iterations	time	time/iter	RMSE y_1	RMSE y_2	BFR y_1	BFR y_2
3	1	5	87	0.4667	0.3141	320	514.19	1.607	0.2816	0.2670	86.03%	83.00%
3	1	8	138	0.4411	0.2979	285	633.59	2.223	0.4557	0.3528	77.39%	77.54%
3	1	10	172	0.3535	0.0295	500	817.81	1.636	0.1133	0.0864	94.38%	94.50%
3	1	15	257	0.3532	0.0252	420	703.28	1.674	0.1145	0.0925	94.32%	94.11%
3	2	3	65	0.3880	0.1733	300	474.93	1.583	0.1622	0.2078	91.95%	86.77%
3	2	5	117	0.3550	0.0728	360	585.42	1.626	0.0994	0.1071	95.07%	93.18%
3	2	7	177	0.4979	0.2764	480	777.75	1.620	0.2942	0.1718	85.41%	89.06%
3	2	10	282	0.3541	0.0255	500	826.19	1.652	0.1188	0.1097	94.11%	93.02%
3	3	3	77	0.4049	0.1898	260	453.32	1.744	0.1494	0.1958	92.59%	87.54%
3	3	5	147	0.4247	0.2683	180	438.12	2.434	0.2694	0.2975	86.64%	81.06%
3	3	7	233	0.6969	0.7338	140	244.47	1.746	0.2452	0.2378	87.84%	84.86%

LSTM network				LSTM Training: Adam BPTT algorithm (GPU)					LSTM Validation			
order	layers	units/layer	# param.	RMSE y_1	RMSE y_2	epochs	time	time/epoch	RMSE y_1	RMSE y_2	BFR y_1	BFR y_2
4	1	2	46	0.5475	0.4164	12000	841.05	0.0701	0.6236	0.7680	69.06%	51.11%
6	1	3	80	0.4142	0.3207	12000	821.17	0.0684	0.5876	0.6221	70.85%	60.40%
8	1	4	122	0.2371	0.1841	12000	1036.00	0.0863	0.4236	0.2769	78.99%	82.37%
10	1	5	172	0.0793	0.0790	12000	827.54	0.0690	0.3811	0.2150	81.09%	86.31%
14	1	7	296	0.0545	0.0505	12000	826.17	0.0688	0.3606	0.2628	82.11%	83.27%
8	2	2	86	0.2747	0.2142	12000	1690.19	0.1408	0.3254	0.2512	83.86%	84.00%
12	2	3	164	0.2131	0.1636	12000	3061.88	0.2552	0.3858	0.4607	80.86%	70.67%
16	2	4	266	0.1781	0.1543	12000	2879.37	0.2399	0.8467	0.4391	58.00%	72.04%
20	2	5	392	0.1867	0.1390	12000	2392.98	0.1994	0.8459	0.7204	58.04%	54.14%
12	3	2	126	0.2046	0.2049	12000	2865.79	0.2388	1.7057	0.3697	15.38%	76.46%
18	3	3	248	0.0755	0.0818	12000	2309.90	0.1925	0.3655	0.1999	81.87%	87.27%

GRU network				GRU Training: Adam BPTT algorithm (GPU)					GRU Validation			
order	layers	units/layer	# param.	RMSE y_1	RMSE y_2	epochs	time	time/epoch	RMSE y_1	RMSE y_2	BFR y_1	BFR y_2
3	1	3	71	0.4960	0.3020	12000	1498.09	0.1248	1.1727	1.3030	41.82%	17.05%
4	1	4	106	0.1376	0.1128	12000	1297.46	0.1081	0.3307	0.2031	83.59%	87.07%
5	1	5	147	0.1617	0.1380	12000	819.22	0.0683	0.1929	0.2127	90.43%	86.46%
7	1	7	247	0.0564	0.0504	12000	810.15	0.0675	0.2219	0.2425	88.99%	84.56%
10	1	10	442	0.0741	0.0853	12000	1460.55	0.1217	0.4643	0.7117	76.96%	54.69%
6	2	3	143	0.2337	0.1584	12000	1578.26	0.1315	0.3226	0.3752	84.00%	76.11%
8	2	4	226	0.1353	0.1265	12000	1581.26	0.1318	0.3751	0.5469	81.39%	65.18%
10	2	5	327	0.0326	0.0309	12000	1591.46	0.1326	0.6165	0.2345	69.41%	85.07%
14	2	7	583	0.0253	0.0325	12000	1571.18	0.1309	0.3244	0.3920	83.91%	75.05%
6	3	2	114	0.1929	0.1647	12000	3638.46	0.3032	0.3943	0.2501	80.44%	84.08%
9	3	3	215	0.0829	0.0858	12000	3741.53	0.3118	0.3664	0.2032	81.83%	87.07%

NNARX network				NNARX Training: Adam BP algorithm (GPU)					NNARX Validation			
order	layers	neuron/layer	# param.	RMSE y_1	RMSE y_2	epochs	time	time/epoch	RMSE y_1	RMSE y_2	BFR y_1	BFR y_2
3	1	5	87	5.0156	4.0211	1000	89.59	0.090	6.3442	3.6032	-214.72%	-129.39%
3	1	8	138	6.8757	6.9953	1000	93.47	0.093	7.2585	6.9879	-260.08%	-344.87%
3	1	10	172	7.8516	7.7647	1000	104.78	0.105	7.7406	9.3001	-284.00%	-492.07%
3	1	15	257	8.0630	9.8919	1000	112.59	0.113	7.4535	10.7121	-269.76%	-581.97%
3	2	3	65	8.2622	9.5509	1000	170.33	0.170	8.1210	9.6828	-302.87%	-516.44%
3	2	5	117	7.7178	9.4936	1000	120.02	0.120	6.6021	9.3484	-227.52%	-495.15%
3	2	7	177	9.9773	8.4243	1000	117.51	0.118	9.8954	8.5393	-390.90%	-443.64%
3	2	10	282	2.5683	5.5859	1000	105.30	0.105	2.0974	5.8676	-4.05%	-273.55%
3	3	3	77	5.4776	3.1718	1000	120.97	0.121	5.5254	2.8112	-174.11%	-78.97%
3	3	5	147	5.3081	5.7561	1000	112.76	0.113	5.2680	6.5923	-161.34%	-319.69%
3	3	7	233	7.6568	9.9372	1000	120.09	0.120	7.5069	11.4208	-272.40%	-627.09%

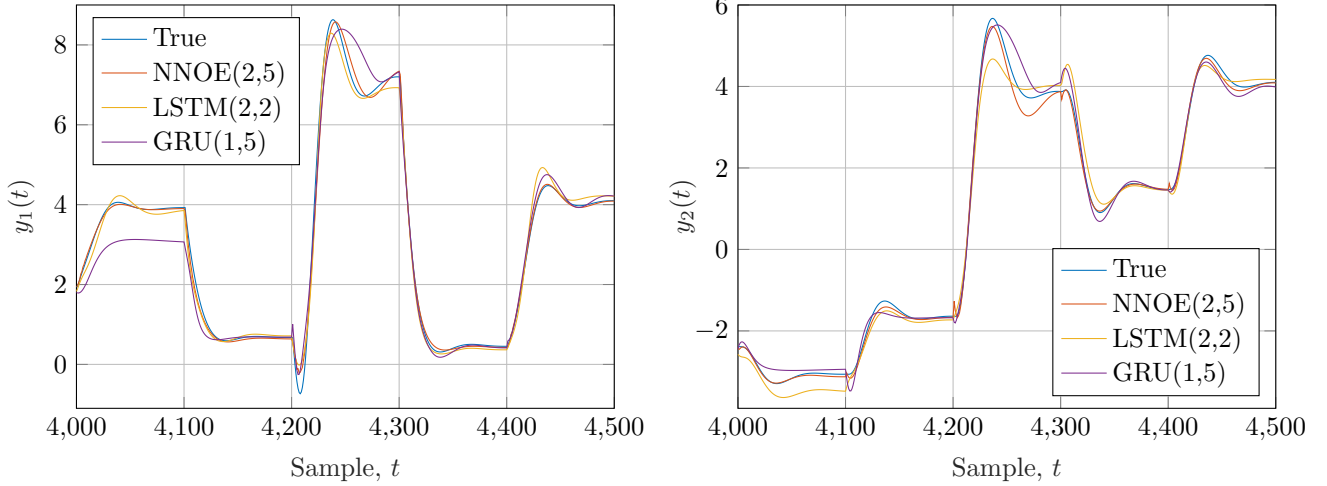


Figure 3: Example 3. Validation output of the top-performing models in each class for output y_1 (left) and y_2 (right).

Table 6: Example 4: Comparison of parameters estimated for the magnetic levitation system using SEM with FL-CMO, SEM with Adam BPTT, and PEM based on LS.

	k_m (H m)	k_0 (N m)
True	2.1039×10^{-4}	0.0
FL-CMO	2.1037×10^{-4}	2.4108×10^{-5}
Adam BPTT	7.46×10^{-4}	-0.143
LS	2.1228×10^{-4}	-3.6130×10^{-4}

Our theoretical analysis provides guarantees of convergence and establishes connections between the proposed approach and the conventional unconstrained formulation. By leveraging the problem structure and employing sparse Q-less QR factorization, we reduce the computational complexity of the iterative process compared to standard unconstrained optimization techniques. Future research will focus on developing solutions to enhance scalability in large-scale problems.

Extensive numerical experiments on black-box and gray-box problems, including system identification benchmarks, reveal that the proposed approach outperforms conventional methods. Additionally, we find that adequately trained neural NIO models can exhibit superior performance compared to state-space neural models such as LSTM and GRU. These findings establish a principled framework for constrained simulation error minimization and offer an efficient alternative to gradient-based identification methods for nonlinear input-output systems.

References

- [Adeoye and Bemporad, 2024] Adeoye, A. D. and Bemporad, A. (2024). An inexact sequential quadratic programming method for learning and control of re-
- current neural networks. *IEEE Trans. Neural Netw. Learn. Syst.*, pages 1–15.
- [Bas et al., 2022] Bas, E., Egrioglu, E., and Kolenen, E. (2022). Training simple recurrent deep artificial neural network for forecasting using particle swarm optimization. *Granul. Comput.*, 7(2):411–420.
- [Baydin et al., 2018] Baydin, A. G., Pearlmutter, B. A., Radul, A. A., and Siskind, J. M. (2018). Automatic differentiation in machine learning: a survey. *J. Mach. Learn. Res.*, 18:1–43.
- [Belz et al., 2017] Belz, J., Münker, T., Heinz, T. O., Kampmann, G., and Nelles, O. (2017). Automatic modeling with local model networks for benchmark processes. In *IFAC World Congress*, volume 50, pages 470–475.
- [Bemporad, 2022] Bemporad, A. (2022). Recurrent neural network training with convex loss and regularization functions by extended kalman filtering. *IEEE Trans. Autom. Control*, 68(9):5661–5668.
- [Bemporad, 2024] Bemporad, A. (2024). Linear and nonlinear system identification under ℓ_1 -and group-Lasso regularization via L-BFGS-B. *arXiv preprint arXiv:2403.03827*.
- [Bengio et al., 1994] Bengio, Y., Simard, P., and Frasconi, P. (1994). Learning long-term dependencies with gradient descent is difficult. *IEEE Trans. Neural Netw.*, 5(2):157–166.
- [Blanco et al., 2001] Blanco, A., Delgado, M., and Pegalajar, M. C. (2001). A real-coded genetic algorithm for training recurrent neural networks. *Neural Netw.*, 14(1):93–105.
- [Bohlin, 2006] Bohlin, T. P. (2006). *Practical grey-box process identification: theory and applications*. Springer Science & Business Media.

- [Cerone et al., 2023] Cerone, V., Fosson, S. M., Pirrera, S., and Regruto, D. (2023). Alternating direction method of multipliers for polynomial optimization. In *Eur. Control Conf. (ECC)*, pages 1–6.
- [Cerone et al., 2024] Cerone, V., Fosson, S. M., Pirrera, S., and Regruto, D. (2024). A new framework for constrained optimization via feedback control of lagrange multipliers. *arXiv preprint arXiv:2403.12738*.
- [Cerone et al., 2014] Cerone, V., Lasserre, J.-B., Piga, D., and Regruto, D. (2014). A unified framework for solving a general class of conditional and robust set-membership estimation problems. *IEEE Trans. Autom. Control*, 59(11):2897–2909.
- [Cerone et al., 2012] Cerone, V., Piga, D., and Regruto, D. (2012). Set-membership error-in-variables identification through convex relaxation techniques. *IEEE Trans. Autom. Control*, 57(2):517–522.
- [Chollet et al., 2015] Chollet, F. et al. (2015). Keras. <https://github.com/keras-team/keras>.
- [Conte et al., 1999] Conte, G., Moog, C. H., and Perdon, A. M. (1999). *Nonlinear control systems: An algebraic setting*, volume 242. Springer.
- [Davis, 2011] Davis, T. A. (2011). Algorithm 915, suitesparseqr: Multifrontal multithreaded rank-revealing sparse QR factorization. *ACM Trans. Math. Softw.*, 38(1):1–22.
- [Esfahani et al., 2017] Esfahani, A. F., Dreesen, P., Tiels, K., Noël, J.-P., and Schoukens, J. (2017). Polynomial state-space model decoupling for the identification of hysteretic systems. In *IFAC World Congr.*, pages 458–463.
- [Farina and Piroddi, 2010] Farina, M. and Piroddi, L. (2010). Convergence properties of an iterative prediction approach to nonlinear sem parameter estimation. In *IEEE Conf. Decis. Control (CDC)*, pages 7226–7231. IEEE.
- [Farina and Piroddi, 2011] Farina, M. and Piroddi, L. (2011). Simulation error minimization identification based on multi-stage prediction. *Int. J. Adapt. Control Signal Process.*, 25(5):389–406.
- [Forgione and Piga, 2021] Forgione, M. and Piga, D. (2021). dynonet: A neural network architecture for learning dynamical systems. *Int. J. Adapt. Control Signal Process.*, 35(4):612–626.
- [Isidori, 1995] Isidori, A. (1995). *Nonlinear Control Systems*. Springer London.
- [Khalil, 2002] Khalil, H. K. (2002). *Nonlinear Systems*. Pearson Education. Prentice Hall, 3rd edition.
- [Laue et al., 2018] Laue, S., Mitterreiter, M., and Giesen, J. (2018). Computing higher order derivatives of matrix and tensor expressions. In *Adv. Neural Inf. Process. Syst. (NIPS)*.
- [Liu et al., 2018] Liu, X., Liu, S., Sha, J., Yu, J., Xu, Z., Chen, X., and Meng, H. (2018). Limited-memory BFGS optimization of recurrent neural network language models for speech recognition. In *Int. Conf. Acoust. Speech Signal Process. (ICASSP)*, pages 6114–6118. IEEE.
- [Ljung, 1999] Ljung, L. (1999). *System Identification: Theory for the User*. Prentice Hall PTR.
- [Medsker and Jain, 1999] Medsker, L. and Jain, L. C. (1999). *Recurrent neural networks: design and applications*. CRC press.
- [Milanese et al., 2013] Milanese, M., Norton, J., Piet-Lahanier, H., and Walter, É. (2013). *Bounding Approaches to System Identification*. Springer US.
- [Milanese and Novara, 2004] Milanese, M. and Novara, C. (2004). Set membership identification of nonlinear systems. *Automatica*, 40(6):957–975.
- [Mirikitani and Nikolaev, 2009] Mirikitani, D. T. and Nikolaev, N. (2009). Recursive bayesian recurrent neural networks for time-series modeling. *IEEE Trans. Neural Netw.*, 21(2):262–274.
- [Narendra and Parthasarathy, 1991] Narendra, K. and Parthasarathy, K. (1991). Gradient methods for the optimization of dynamical systems containing neural networks. *IEEE Trans. Neural Netw.*, 2(2):252–262.
- [Noel and Schoukens, 2016] Noel, J.-P. and Schoukens, M. (2016). Hysteretic benchmark with a dynamic nonlinearity. In *Workshop on nonlinear system identification benchmarks*, pages 7–14.
- [Nørgård et al., 1996] Nørgård, P. M., Ravn, O., Hansen, L. K., and Poulsen, N. K. (1996). The nnsysid toolbox - a matlab toolbox for system identification with neural networks. In *IEEE Symp. Comput.-Aided Control Syst. Des.*, pages 374–379. IEEE.
- [Parrilo and Ljung, 2003] Parrilo, P. A. and Ljung, L. (2003). Initialization of physical parameter estimates. In *IFAC Symp. Syst. Identif. (SYSID)*, pages 1483–1488.
- [Pascanu et al., 2013] Pascanu, R., Mikolov, T., and Bengio, Y. (2013). On the difficulty of training recurrent neural networks. In *Int. Conf. Mach. Learn. (ICML)*, pages 1310–1318.
- [Peng and Magoulas, 2011] Peng, C.-C. and Magoulas, G. (2011). Nonmonotone BFGS-trained recurrent neural networks for temporal sequence processing. *Appl. Math. Comput.*, 217(12):5421–5441.
- [Piroddi, 2008] Piroddi, L. (2008). Simulation error minimisation methods for narx model identification. *Int. J. Model. Identif. Control*, 3(4):392–403.
- [Piroddi and Spinelli, 2003] Piroddi, L. and Spinelli, W. (2003). An identification algorithm for polynomial narx models based on simulation error minimization. *Int. J. Control*, 76(17):1767–1781.

- [Prot and Mercère, 2020] Prot, O. and Mercère, G. (2020). Combining linear algebra and numerical optimization for gray-box affine state-space model identification. IEEE Trans. Autom. Control, 65(8):3272–3285.
- [Ramaswamy, 2023] Ramaswamy, A. (2023). Gradient clipping in deep learning: A dynamical systems perspective. In Int. Conf. Pattern Recognit. Appl. Methods (ICPRAM), volume 1, pages 107–114.
- [Ruder, 2016] Ruder, S. (2016). An overview of gradient descent optimization algorithms. arXiv preprint arXiv:1609.04747.
- [Salem, 2022] Salem, F. M. (2022). Recurrent Neural Networks. Springer.
- [Sjöberg et al., 1994] Sjöberg, J., Hjalmarsson, H., and Ljung, L. (1994). Neural networks in system identification. In IFAC Symp. Syst. Identif. (SYSID), pages 359–382.
- [Söderström and Stoica, 1982] Söderström, T. and Stoica, P. (1982). Some properties of the output error method. Automatica, 18(1):93–99.
- [Stewart, 1998] Stewart, G. W. (1998). Matrix algorithms: volume 1: basic decompositions. SIAM.
- [Sundnes, 2024] Sundnes, J. (2024). Solving Ordinary Differential Equations in Python. Springer Nature Switzerland.
- [Wang et al., 2009] Wang, J., Sano, A., Chen, T., and Huang, B. (2009). Identification of hammerstein systems without explicit parameterisation of nonlinearity. Int. J. Control, 82(5):937–952.
- [Wanner and Hairer, 1996] Wanner, G. and Hairer, E. (1996). Solving ordinary differential equations II, volume 375. Springer Berlin Heidelberg New York.
- [Williams and Zipser, 1990] Williams, R. J. and Zipser, D. (1990). Gradient-based learning algorithms for recurrent connectionist networks. Citeseer.
- [Zhang, 2004] Zhang, Q. (2004). Nonlinear system identification with output error model through stabilized simulation. In IFAC Symp. Nonlinear Control Syst. (NOLCOS), pages 501–506.